International Journal of Biological Macromolecules 152 (2020) 709–717

Contents lists available at ScienceDirect

International Journal of Biological Macromolecules

journal homepage: http://www.elsevier.com/locate/ijbiomac

Inhibitory activity of biofunctionalized silver-capped *N*-methylated water-soluble chitosan thiomer for microbial and biofilm infections

Reda F.M. Elshaarawy [a,b,*], Lamia A. Ismail [c], Mohammad Y. Alfaifi [d], Moustafa A. Rizk [e,f], Enas E. Eltamany [g], Christoph Janiak [b,**]

[a] Department of Chemistry, Faculty of Science, Suez University, 43533 Suez, Egypt
[b] Institut für Anorganische Chemie und Strukturchemie, Heinrich-Heine Universität Düsseldorf, Düsseldorf, Germany
[c] Department of Chemistry, Faculty of Science, Port Said University, Port Said, Egypt
[d] Biology Department, Faculty of Science, King Khalid University, 9004 Abha, Saudi Arabia
[e] Chemistry Department, College of Science and Arts-Sharurah, Najran University, Sharurah, Saudi Arabia
[f] Department of Chemistry, Faculty of Science, Suez Canal University, Ismailia, Egypt
[g] Department of Pharmacognosy, Faculty of Pharmacy, Suez Canal University, Ismailia, Egypt

ARTICLE INFO

Article history:
Received 7 January 2020
Received in revised form 24 February 2020
Accepted 25 February 2020
Available online 28 February 2020

Keywords:
Methylated chitosan thiomer
Silver architectures
Antibacterial and anti-biofilm

ABSTRACT

One of the most important self-defense strategies employed by bacteria to resist the action of antibiotics is a biofilm formation upon the infected surface. Thus, there is an urgent need to explore novel candidates that have potent antibacterial and anti-biofilm effects to tackle this challenge. In this endeavor, we have transformed shrimp shell wastes to *N*-methylated water-soluble chitosan thiomer (MWSCT) which was used as either a chelating agent or bio-reductant and capping agent for Ag(I) ions in the preparation of a Ag(I)MWSCT complex or silver nanocomposite (Ag(0)MWSCT), for targeting antibacterial and anti-biofilm applications. The antibacterial and anti-biofilm performance of the new methylated chitosan thiomer (MWSCT) and its silver architectures (Ag(I) MWSCT, Ag(0)MWSCT) were assessed in vitro against *E. coli* and *S. aureus*. These new materials have significant capacities to synergistically inhibit the proliferation of the targeted bacterial cells and biofilm formation, in a structure- and species-dependent manner. Ag(0)MWSCT emerged as the most potent compound in inhibiting the growth of bacterial strains ($MIC_{E.\ coli}$/ $MIC_{S.\ aureus}$ = 0.05/ 0.34 μg/mL, 1.6-/ 2.5-times lower than that recorded for the clinical drug (ciprofloxacin, Cipro). Also, this nanocomposite showed the highest anti-biofilm effects (only 1.7% *E. coli* biofilm growth; 11.8% *staphylococcal* biofilm growth).

1. Introduction

Fighting bacterial colonization and biofilm formation (self-secreted extracellular polymeric matrices comprising exopolysaccharides (EPS), DNA, and lipid) remains a major challenge in many domains including the medical, environmental, and industrial fields [1,2,3]. Biofilms can frequently establish on living tissues, synthetic biomaterials (such as urinary catheters, dental implants, and arthro-prostheses) and abiotic solid surfaces, causing serious health and environmental problems [1,2,3]. Meanwhile, the embedding of bacterial pathogens in biofilms alters their behaviors comparing to planktonic bacteria, such as acquiring high resistance to antibiotics and stress coupled with the host's immune defense [4]. Several innovative strategies have been developed recently to combat biofilms. One strategy exploits self-secreted ingredients of a biofilm to damage biofilms through attacking its EPS matrix, nevertheless, this strategy could not kill biofilm-inducing bacterial cells [5,6,7]. Another strategy is to utilize nano-scaffolds to deliver antibiotics to the core of biofilms allowing them to freely access and affect bacterial cells resulting in their death and biofilm eradication [8,9]. This strategy offers an opportunity to minimize antibiotic dosage required for biofilm extermination. However, the reliance on traditional antibiotics in this strategy may foster the onset of acquired antibiotic-resistance. Another more recent strategy is to design novel smart antimicrobial materials that have the capacity to kill bacterial cells and destroy biofilms because of their prominent bioactivity [10,11,12,13].

Amongst these antimicrobial materials, silver nanoparticles (AgNPs) occupy a forefront as potent antimicrobial agents that exhibit broad-spectrum toxicity against diverse microorganisms. Moreover, AgNPs have a lower propensity to induce bacterial resistance in comparison with traditional antibiotic treatments [14,15,16]. Hence, AgNPs have been broadly used in therapeutic catheters, prosthetic cardiac, and

* Correspondence to: R. F. M. Elshaarawy, Department of Chemistry, Faculty of Science, Suez University, 43533 Suez, Egypt.
** Corresponding author.
E-mail addresses: reda_elshaarawi@science.suez.edu.eg, Reda.El-Shaarawy@uni-duesseldorf.de (R.F.M. Elshaarawy), janiak@uni-duesseldorf.de (C. Janiak).

https://doi.org/10.1016/j.ijbiomac.2020.02.284
0141-8130/

orthopedic devices [17,18]. Furthermore, it was reported that AgNPs exhibited some potential as anti-biofilm agents [19,20,21]. Interestingly, the antimicrobial efficacy for AgNPs is greatly depending on particle size. Many researchers reported that AgNPs with sizes >20 nm are not optimal for the antimicrobial applications [22]. Whereas, AgNPs of particle sizes ≤20 nm were recognized as the most potent antibacterial nanoparticles due to their ability to directly interact with bacterial cells [23]. Nevertheless, the biomedical applications of AgNPs are often disappointing due to the ease of their oxidation and agglomeration into bulky particles or fibers, resulting in the loss of their biological features along with the acquisition of harmful properties for the environment and human health [24,25]. Thus, searching for safe, smart, and innovative stabilizers for wrapping AgNPs is an important issue to address these challenges. Enveloping of AgNPs is an excellent technique to preserve and boost their features as it increases the stability of AgNPs and decreases their agglomeration. Furthermore, this wrapping technique is important to block the cytotoxic action of AgNPs toward living cells.

Despite several organic and inorganic coating materials which have been used to stabilize AgNPs, the biodegradable biopolymer, chitosan, and its derivatives have been proven to be more effective in stabilizing AgNPs and maintaining their morphological properties which play pivotal roles in their antimicrobial action [26,27]. Particularly, water-soluble chitosan (WSC) is considered as the most attractive bioactive-encapsulating agent where the aqueous-solubility of WSC enhances its digestion, absorption and thus bioavailability [28]. Furthermore, the therapeutic potentials of WSC such as an antimicrobial [29,30], anticancer agent [31], antioxidant [32,33] etc., were emphasized. Furthermore, the silver-tagged chitosan nanocomposites were demonstrated excellent antimicrobial performance [34,35].

The aforementioned prominent facts coupled with our ongoing interest in searching for promising chitosan-based pharmaceutical materials [36,37,38] motivated us to design a facile and efficient protocol for the green synthesis and bio-functionalization of AgNPs (≤ 20 nm) mediated by *N*-methylated water-soluble chitosan thiomer (MWSCT) to give novel MWSCT-based Ag(I) complex (Ag(I)MWSCT) and silver nanocomposite (Ag(0)MWSCT) for targeting antibacterial and anti-biofilm applications.

2. Experimental section

Details for the chemicals and different analytical techniques used for the comprehensive characterization of as-synthesized materials were described in the electronic supplementary material (**ESM**). Moreover, extraction of chitosan from shrimp shell and its controllable degradation into low molecular weight chitosan (LWMC), *N*,*N*-dimethyl water-soluble chitosan (DMWSC), *N*,*N*,*N*-trimethyl water-soluble chitosan (TMWSC) and *N*-methylated water-soluble chitosan thiomer (MWSCT) were also given in **ESM**.

2.1. Synthesis of Ag(I)MWSCT complex

To a hot solution of MWSCT (0.1 g, 0.65 mmol of thiol group) in 50 mL of ethanol containing a few drops of ammonium hydroxide, a hot solution of silver(I) nitrate (0.11 g, 0.65 mmol) in 25 mL of deionized (DI) water was added dropwise. The Ag(I) complex was precipitated immediately from the reaction mixture as a gray precipitate. Then, the solution was stirred at room temperature (RT) for 1 h. Thereafter, the Ag(I)MWSCT was collected by filtration, washed with cold ethanol followed by Et_2O and dried in vacuo. Yield 83%.

2.2. Synthesis of Ag(0)MWSCT nano-composite

MWSCT-silver nano-composite was synthesized according to earlier reported work [39] with a slight change. Briefly, 0.1 g of MWSCT (0.65 mmol of thiol group) was dissolved in 50 mL of DI water at 60–65 °C and the acidity of this solution was adjusted to pH 5.0 using 1% $AcOH_{aq}$. Then, a hot solution of $AgNO_3$ in DI water (10 mL, 1 mM) was slowly added to MWSCT solution under vigorous stirring. A gradual change in the color of the reaction mixture from pale yellow to dark yellow and eventually to reddish-brown was observed upon the gradual addition of $AgNO_3$ to the thiomer solution. The reaction was further stirred under reflux conditions for 1 h to ensure completeness of reaction. The resulting reddish-brown suspension of the nano-composite was centrifuged and Ag(0)MWSCT was collected and dried in vacuo at 50 °C. Yield 34%.

2.3. Antibacterial studies

The bacterial species used in this work, *Staphylococcus aureus* (*S. aureus*, ATCC 29737) and *Escherichia coli* (*E. coli*, ATCC 10536) were obtained from the National Organization for Drug Control and Research (NODCAR), Cairo, Egypt. All bacterial species were grown aerobically in a nutrient broth (NB; Difco) containing sterile glycerol (50%) kept at −70 °C. These strains were sub-cultured twice in NB and incubated at 37 °C for further use.

2.3.1. Agar well-diffusion (AWD) method

The antibacterial performance of synthesized MWSC thiomer (MWSCT), its silver derivatives (Ag(I)MWSCT, Ag(0)MWSCT) and ciprofloxacin HCl (Cipro) (positive control) were assessed for their capacity to inhibit the growth of broth cultured *E. coli* and *S. aureus* using the agar well-diffusion (AWD) method [40]. Three different concentrations of the materials (25, 50 and 150 μg/mL) were tested against the pathogenic bacterial strains. 20 mL of the nutrient agar was poured into Petri dishes and left to solidify, thereafter, wells were constructed using gel puncture and filled with three different concentrations of the tested compounds (30 μL) in three different wells. The zones of inhibition (ZOI, mm), the clear zone around the wells (see **Fig. S1**), were measured as a marker of antibacterial activity.

2.3.2. Colony forming unit (CFU) method

The antimicrobial activities of MWSCT-based silver architectures (Ag(I)MWSCT, Ag(0)MWSCT) and Cipro were screened against *E. coli* and *S. aureus* by the CFU method. This experiment was performed using a set of three test tubes for each sample. In the foremost tube, a mixture of nutrient broth (NB) (10 mL) and bacterial culture (1.0 mL) was added. The second test tube (treatment tube) contains a mixture of NB (10 mL), bacterial culture (1.0 mL), and a solution of the tested sample (50 μg/mL). The last test tube was filled with a mixture of NB (10 mL) and a sample (50 μg/mL). Then, 3 mL suspension from each sample was diluted to produce an operating (growth control) suspension of 19.3×10^6 and 21.5×10^6 CFU/mL for *S. aureus* and *E. coli*, respectively. Thereafter, all test tubes were incubated under shaking for 24 h at 30 °C. Afterward, 20 μL of each diluted suspension was added to the agar medium and kept in an incubator at 37 °C for 24 h. Then, the CFU/mL for each plate was examined using the plate count method. The percentage of bacterial colonies reduction (R%) was calculated by the following equation (**Eq. 1**):

$$\mathbf{R}\% = \frac{BC_{CT} - BC_{TT}}{BC_{CT}} \quad (1)$$

where BC_{CT} and BC_{TT} are the number of bacterial colonies in growth control and treatment test tubes, respectively.

2.4. Determination of MIC

The minimum inhibitory concentration (MIC), the lowest concentration blocking the growth of visible bacterial cells at the bottom of well, of MWSCT-based silver architectures (Ag(I) MWSCT, Ag(0)MWSCT) and Cipro against *E. coli* and *S. aureus* cells was determined by a standard

serial dilution experiment in a 96-well microtiter plate. Briefly, nine-fold serial dilutions (starting from 32 μg/mL) of MWSCT and its silver derivatives were prepared in Mueller-Hinton broth (MHB) and transferred to a 96-well plate (50 μL/well). Afterward, the overnight-cultivated bacterial culture was diluted with MHB to ~10^6 CFU/ mL and then 50 μL of each diluted culture was added to each well. Thereafter, all plates were incubated for 24 h at 37 °C before the estimation of MIC values which determined macroscopically by comparison of the bacterial growth in the tested wells to the growth control (pure untreated bacterial culture).

2.5. Anti-biofilm study

The anti-biofilm assay of the new compounds was carried out according to our previously reported work [41] with slight modification. Briefly, flat-bottom 96-well microtiter plates coated with aqueous sample solution (10 μg/mL, 30 μL/ well) were left to dry overnight at 37 °C. DI water was used as a negative control. *S. aureus* and *E. coli* were cultivated on tryptic soy agar (TSA) overnight at 37 °C. Then, a few colonies of each bacterial species were suspended in a tryptic soy broth supplemented with 2% glucose (TSB). Thereafter, the suspension was vortexed for 60 s and its optical density at 600 nm ($OD_{600\ nm}$) was adjusted to be 0.08 which is matching for ~10^7 CFU/ mL. Afterward, 200 μL of the diluted bacterial suspensions were added to each pre-coated well. Non-inoculated TSB medium was served as a growth control. Eventually, plates were incubated at 37 °C for 24 h. Subsequently, quantification of biofilms was performed using the crystal violet staining protocol [42]. Briefly, the plates were rinsed three times with phosphate-buffered saline (PBS, pH = 7.4) and air-dried. Then, each well was stained with crystal violet solution (0.1% (v/v), 200 μL) at RT for 15 min. Afterwards all wells were washed three times with PBS, and then 200 μL of ethanol were added to each well and incubated at RT for 30 min to solubilize the dye. Finally, the absorbance was measured using a microplate reader at 600 nm.

2.6. Statistical analysis

The SPSS 20.0 software (SPSS Inc.) was used for all statistical assessments. Data were analyzed using one-way variance (ANOVA) followed by a multi-range test Tukey's. All results were presented as mean ± standard medium error and significance level was considered with P values <0.05.

3. Results and discussion

3.1. Chemistry

Multiple integrated thermochemical processes including deproteination, demineralization, deacetylation, oxidative degradation, *N*-methylation, and thiolation were followed to convert shrimp-shells wastes into low molecular weight chitosan (LWMC), *N*-methylated water-soluble chitosan (MWSC) and *N*-methylated water-soluble chitosan thiomer (MWSCT) (Schemes 1). Initially, shrimp-shells wastes were refined into chitin (Ch) which undergoes partial acetylation forming chitosan, followed by oxidative degradation mediated by H_2O_2 to form LMWC [37].

Then a water-soluble *N,N,N*-trimethyl derivative of LMWC (MWSC) was obtained by quaternization of chitosan using dimethyl carbonate ($(CH_3)_2CO_3$) as *N*-methylation reagent in 1-butyl-3-methylimidazolium chloride ([bmim]Cl) ionic liquid [43]. Afterward, the MWSC was subjected to an indirect thiolation process by reaction with thiourea in an acidic medium under microwave condition to form the isothiouronium ion intermediate, followed by microwave-assisted alkaline-hydrolysis to generate MWSCT [44].

Then, the as-synthesized *N*-methylated chitosan thiomer was used as either a chelating agent for Ag(I) ions to prepare the Ag(I)-chitosan-thiolate complex (Ag(I)MWSCT), or as a reducing, stabilizing, and capping agent for elemental nanosilver Ag(0) in the synthesis of Ag(0)-chitosan-thiomer nanocomposite (Ag(0)MWSCT) (Schemes 2). The newly synthesized materials were characterized using different spectroscopic and microscopic techniques.

3.2. Structural characterizations

The molecular weights (M_w) of those chitosan derivatives were estimated from the intrinsic viscosities ([η]) values, for their aqueous CH_3COOH/ NaCl solutions at 25 °C, based on Mark–Houwink–Sakurada

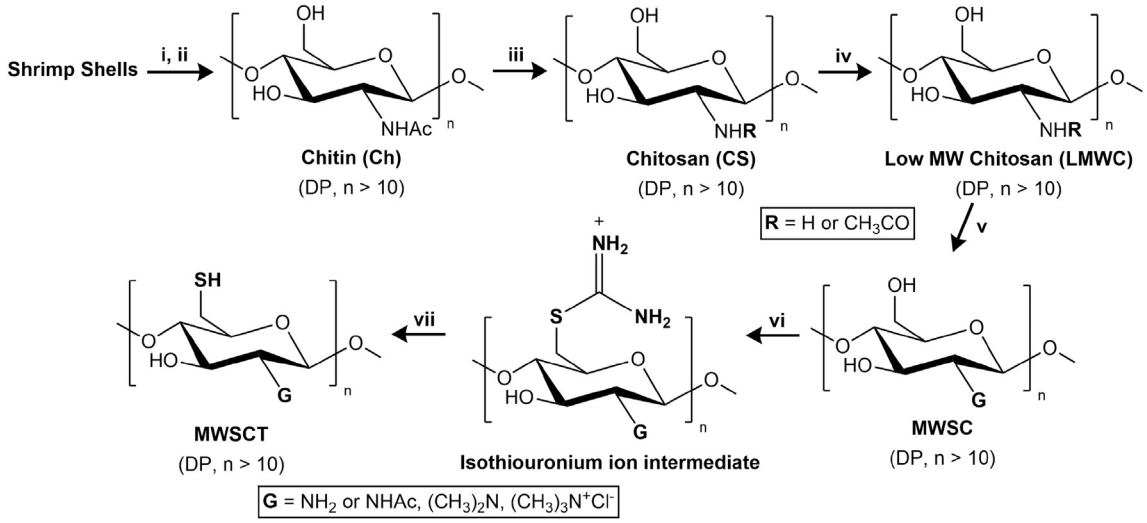

i- Deproteination: 1 M NaOH, stirring, 65°C, 90 min**; ii- Demineralization:** 0.75 M HCl, stirring, RT, 150 min**;** **iii- Deacetylation:** (**a**) 50% NaOH, stirring, 100 °C, 12 h. (**b**) 50% NaOH, reflux, 1 h, H2O, 80 °C **; iv- Oxidative degradation:** H_2O_2 30% (4.4%)**,** stirring, 30 °C, 1.5 h; **v- *N*- Methylation**: (**a**) HCOOH/ HCHO, reflux, 5 days, (**b**) [bmim]Cl, stirring, 100 °C, 3 h, $(CH_3)_2CO_3$, stirring, 150 °C, 3.5 h; **vi, vii- thiolation**: (**vi**) Thiourea, HCl, microwave (640 W), 5 min,(**vii**) 0.2 NaOH,, microwave (640 W), 90 sec, 0.1 M HCl.

Scheme 1. Consecutive reaction pathway for the preparation of chitin, chitosan, LMWC, MWSC and MWSCT.

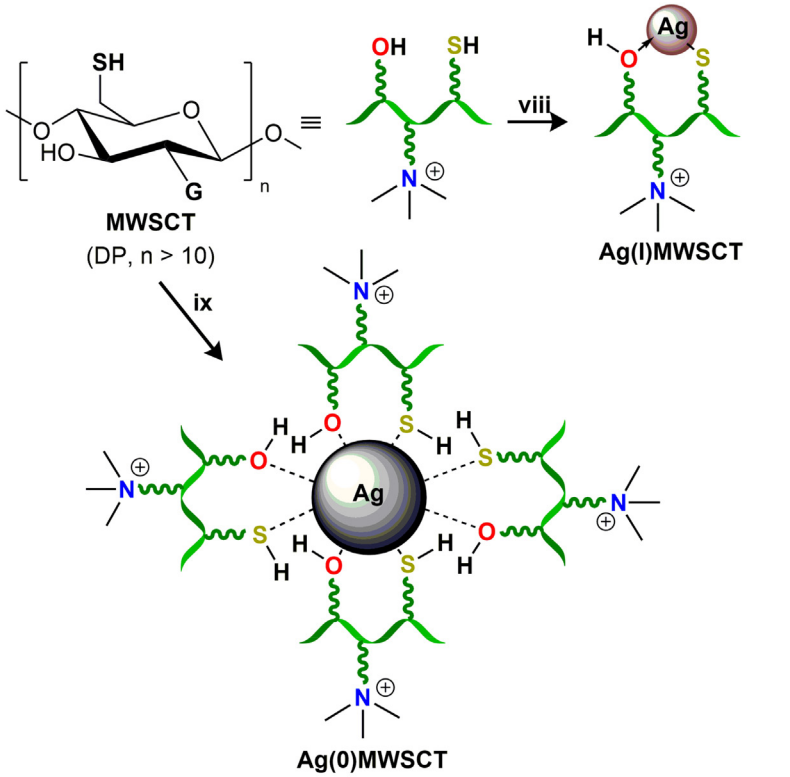

Scheme 2. Protocol for biofunctionalization of silver motifs with *N*-methylated water-soluble chitosan thiomer (MWSCT).

(MHS) equation [45]; $[\eta] = k.M^{\alpha}$ where η intrinsic viscosity, $k = 1.81 \times 10^{-3}$ (cm^3/g) and $\alpha = 0.93$. Table 1 shows the intrinsic parameters (viscosity ($[\eta]$), molecular weight (M_w), elemental analysis (EA), degree of aceylation/quaternization (DA/DQ) and degree of substitution (DS) of chitosan derivatives).

The FTIR spectra of LMWC, MWSC, MWSCT, Ag(I)MWSCT, and Ag(0) MWSCT (Fig. 1), offer initial evidence for the success of our synthesis protocol in obtaining the new desired materials. The main characteristic peaks for LMWC were observed at 3463, 1653, and 1581 cm^{-1} attributable to the stretching vibrations of O—H and N—H, amide I (C=O), N—H bending (NH_2) and amide II, respectively [41,46]. On the other hand, the disappearance of the N—H absorption band at 1592 cm^{-1} in the spectrum of MWSC confirms the replacement of H-atoms in the amino group by the methyl group and quaternization of the N-atom of LMWC [47]. Thiolation of MWSC to form MWSCT is evident by the emergence of new absorption bands at 2685 and 638 cm^{-1} in the spectrum of MWSCT, corresponding to S—H and C—S stretching vibrations of thiol group [39,44]. Compared to the FTIR spectrum of MWSCT, the spectrum of the Ag(I)MWSCT complex exhibits the majority of main peaks of MWSCT, nevertheless, a slight peak-shift and/or peak-weakening were observed in a few peaks. For instance, a decrease in the broadness and intensity of the O—H peak coupled with its slight displacement (~3460 cm^{-1}) proves the involvement of the –OH group in complexation with Ag(I) ions. Meanwhile, disappearance of the S—H absorption band (2685 cm^{-1}) coupled with a C—S peak-shift (~635 cm^{-1}) and the emergence of a new peak at 538 cm^{-1} due to

Table 1
Intrinsic physicochemical parameters of chitosan derivatives.

Compd.	$[\eta]$ (mL/g)	M_w (KDa)	EA (%)				DA[a]	DQ[b]	DS[c]
			C	H	N	S			
CS	502.76	713.6	40.63	7.12	7.31	–	24.3	–	–
LMWC	21.83	24.5	40.95	7.20	7.35	–	25.1	–	–
MWSC	36.56	42.6	49.35	8.05	6.29	–	–	12.8	–
MWSCT	40.69	47.8	43.64	7.53	5.21	22.8	–	–	1.49

[a] The degree of acetylation (DA) was calculated from elemental analysis (EA) according to the following equation (Hu et al., 2007): $DA = [(C/N - 5.14)/1.72] \times 100\%$.
[b] The degree of substitution (DS) was calculated from the sulfur content (S%) in the thiomer derivative, according to equation (Eq. (3)), outlined later.
[c] The degree of quaternization (DQ) of MWSC was quantified from the ^1H NMR spectrum based upon equation (Eq. (2)), outlined later.

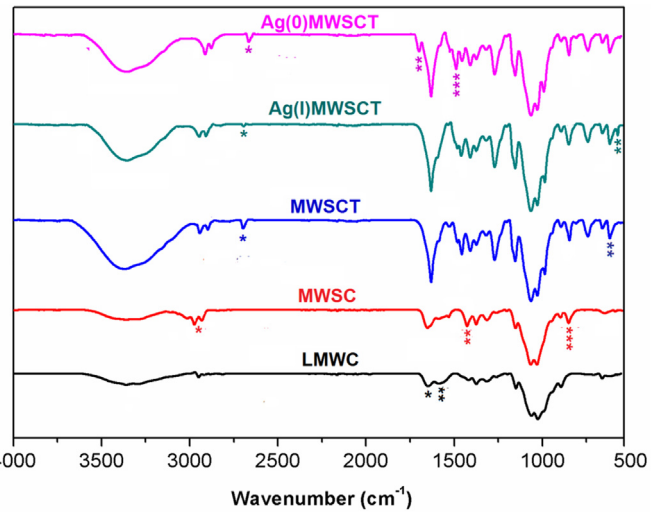

Fig. 1. FTIR spectra for low molecular weight chitosan (LMWC), *N*-methylated water soluble chitosan thiomer (MWSCT), MWSCT-based Ag(I) complex (Ag(I)MWSCT), and silver nano-composite (Ag(0)MWSCT). Peaks assignment: *, amide I (C=O); **, N—H (NH_2), amide II; *,**,***, C—H (CH_3); *, S—H (thiol); **, C-S; *, S—H (thiol); **, Ag-S; *, S—H (thiol); **, C=O; ***, Ag(0).

vibration of the Ag—S moiety confirms the complete deprotonation of a thiol group to give the thiolate anion which shares in coordination to Ag (I) ions [48]. Also, comparing the FTIR spectrum for Ag(0)MWSCT with that of MWSCT reveals a remarkable reduction coupled with slight shifts in the O—H and S—H stretches due to the participation of these groups in the bio-reduction of Ag(I) ions and capping of nanosilver. Noteworthy, the growth of the new peak at 1678 cm^{-1} which can be assigned as a C═O stretching vibration gives evidence for the oxidation of the glycosidic hydroxyl group during Ag(I) reduction [49]. Moreover, the emergence of a new intense peak at 1449 cm^{-1} in the Ag(0)MWSCT spectrum, characteristic for nanosilver, provides evidence for the formation of nanosilver capped with MWSCT [39].

The ^{1}H NMR spectra of LMWC, MWSC, and MWSCT are depicted in Fig. 2. In comparison to the spectrum of LMWC, there are two new singlet peaks at 3.18 ppm (~6H) and 3.84 ppm (2.6H) assigned to the dimethyl- and quaternized-amino groups, respectively. Thus, MWSC comprises a hybrid structure of mainly dimethyl-amino groups with a moderate contribution of quaternized-amino groups, being fully consistent with previously reported work [43]. Moreover, the degree of quaternization (DQ) of MWSC can be quantified from the ^{1}H NMR spectrum based upon Eq. (2) [50]:

$$\mathbf{DQ}\% = \frac{\frac{I_{TMC}}{9}}{I_{H_1}} \times 100 \quad (2)$$

where I_{TMC} and I_{H1} are the integrals of the H-atoms belonging to the quaternized-amino group and the anomeric C-atom (C-1) of the glucopyranose ring. Therefore, the DQ of MWSC was found to be 12.8%.

Compared to the ^{1}H NMR spectrum of MWSC, the spectrum of chitosan—thiomer (MWSCT) shows a new additional intense singlet at 2.77 ppm due to the resonance of the proton of a high-density thiol group (—SH). This sharp signal suggests the competence of our applied thiolation protocol. Moreover, the fluctuations in the intensity and/or chemical shift of peaks provide additional support for the thiolation of MWSC.

The efficiency of the applied thiolation protocol was assessed based on the degree of substitution (DS) (the average number of hydroxyl groups that have been exchanged by the substituent (thiol group) in the anhydrous glucose unit of the monomeric unit for MWSC). The DS values can be calculated from the sulfur content (S%) in the thiomer derivative, which can be estimated using microanalytical and gravimetric techniques, according to Eq. (3) [51]:

$$\mathbf{DS} = \frac{162 \text{ x } S\%}{[100 \text{ x } B] - [(C-1) \text{x } S\%]} \quad (3)$$

where 162 is the molecular weight of the anhydrous glucose unit, B is the atomic weight of sulfur (32 g/mol), C is the molecular weight of the thiol group (33 g/mol). In the analytical estimation by iodometric titration, the sulfur content was found to be 22.6% which is corresponding to DS of 1.5. Meanwhile, the microanalytical analysis supported 22.8% (DS = 1.49).

The success of our proposed protocol for the coordination and/or the bio-reduction of Ag^+ ions into nanosilver mediated by MWSCT can be checked using UV–Vis spectroscopy. The color-change of the colorless MWSCT solution into yellowish-gray (in case of complexation) and reddish-brown (in case of nanosilver formation) upon mixing with $AgNO_3$ indicates the alteration of the microstructure of silver due to coordination or bio-reduction and capping with the MWSCT (Fig. 3). The UV–Vis absorption spectrum of the Ag(I)MWSCT complex is characterized by three distinctive peaks at 381, 459 and 583 nm. As previously

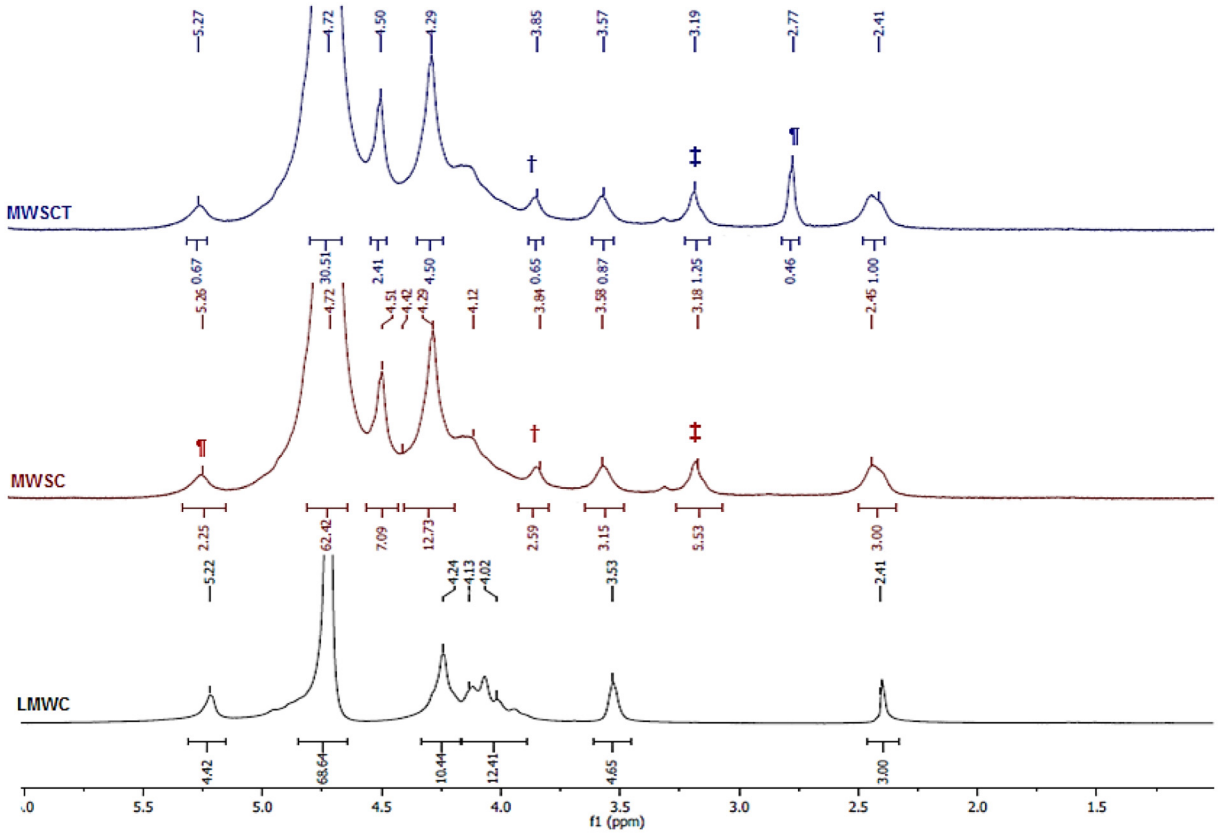

Fig. 2. ^{1}H NMR spectra of LMWC, MWSC and MWSCT solutions in D_2O at 300 MHz, new blue line-framed peaks are due to the nuclear resonance of lactyl protons. Peaks assignment: †, †, quaternized-amino group ($(CH_3)_3N^+$–); ‡, ‡, dimethyl-amino group ($(CH_3)_2N$–); ¶, anomeric C-atom (C-1) of the glucopyranose ring; ¶, S—H (thiol).

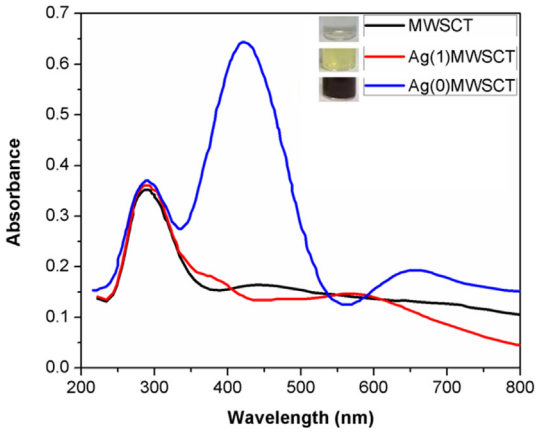

Fig. 3. Comparative UV–Vis spectra of *N*-methylated water soluble chitosan thiomer (MWSCT), MWSCT-based Ag(I) complex (Ag(I)MWSCT), and silver nano-composite (Ag(0)MWSCT).

reported, the broad peak observed at 583 nm is characteristic for Ag(I)-thiolate complexes [52,53] as a result of the deprotonation of the thiol group to give the thiolate anion which then coordinates with Ag(I) ions. On the other hand, the shoulders observed at 381 and 459 nm can be attributed to the absorption by silver clusters, that formed by aggregation of Ag(I) ions (4–9) on the surface of MWSCT as a preliminary step for starting the bio-reduction of Ag(I) ions to Ag(0) atoms [52,53]. As compared to the UV–Vis spectra of MWSCT and Ag(I)MWSCT, the spectrum of Ag(0)MWSCT exhibited a distinctive intensive peak at 423 nm assignable to the surface plasmon resonance (SPR) phenomena characteristic for the metallic nanosilver [54]. Furthermore, the emergence of a new broad band at ~653 nm coupled with the parent peak of MWSCT at ~295 nm gives a strong indication for the formation of nanosilver capped with MWSCT.

To further validate the bio-reduction of Ag(I) to nanosilver (Ag(0)) and its capping with MWSCT, a sample of the obtained product was analyzed using energy-dispersive X-ray (EDX) technique as depicted in Fig. 4E. The EDX spectrum exhibits intense silver peaks around ~3 keV, which is typical for silver crystallites. Moreover, it is clearly observed several peaks for nitrogen, oxygen, carbon, chlorine, and sulfur, which could be assigned to MWSCT bound to the surface of nanosilver.

3.3. Morphological characterizations

The morphological features of MWSCT, Ag(I)MWSCT complex and silver nano-composite (Ag(0)MWSCT) were investigated using SEM and TEM techniques (Fig. 4A-D). It is evident from the SEM micrograph (Fig. 4A) that the MWSCT has a lamellar texture which acquires dislocations upon coordination with Ag(I) ion (Fig. 4B). On the other hand, it is noticed in the SEM micrograph of Ag(0)MWSCT (Fig. 4C) that the silver nanoparticles were randomly distributed onto the surface of MWSCT, confirming a successful preparation of the desired material. It is also noted that nanoparticles agglomerates as the population of metallic Ag in the film were increased. These Ag agglomerates were observed to be unevenly dispersed in the MWSCT matrix. TEM images of the as-synthesized Ag(0)MWSCT (Fig. 4D) revealed that a lower concentration of AgNPs with almost spherical shape and approximate size in the range of 9–15 nm have been scattered in the texture of MWSCT.

3.4. Antibacterial studies

Recently, Chauhan et al. [39] reported that the silver-tagged chitosan-thiomer (CHH–SH–Ag) nanocomposites exhibited promising antibacterial efficacy against *E. coli* and *S. aureus* even at very low concentrations (30–180 μg/mL). Where the CHH–SH–Ag-13 shows the highest ZOI size of 35 mm and lowest MIC 3.7 μg/mL against *E. coli*. Taking into account the previous study, the antibacterial assessment by an AWD experiment, using very low concentrations (25–150 μg/mL), demonstrates superb activity against tested bacterial strains (*S. aureus* and *E. coli*). In general, the efficacy of MWSCT to inhibit the growth of *S. aureus* (ZOI = 18–21 mm) is slightly higher than its activity against *E. coli* (ZOI = 16–18 mm). On the other hand, the ZOIs of new Ag-based MWSCT derivatives were in the ranges of 39–24 and 29–23 mm against *E. coli* and *S. aureus*, respectively, (Fig. 5) confirming that these

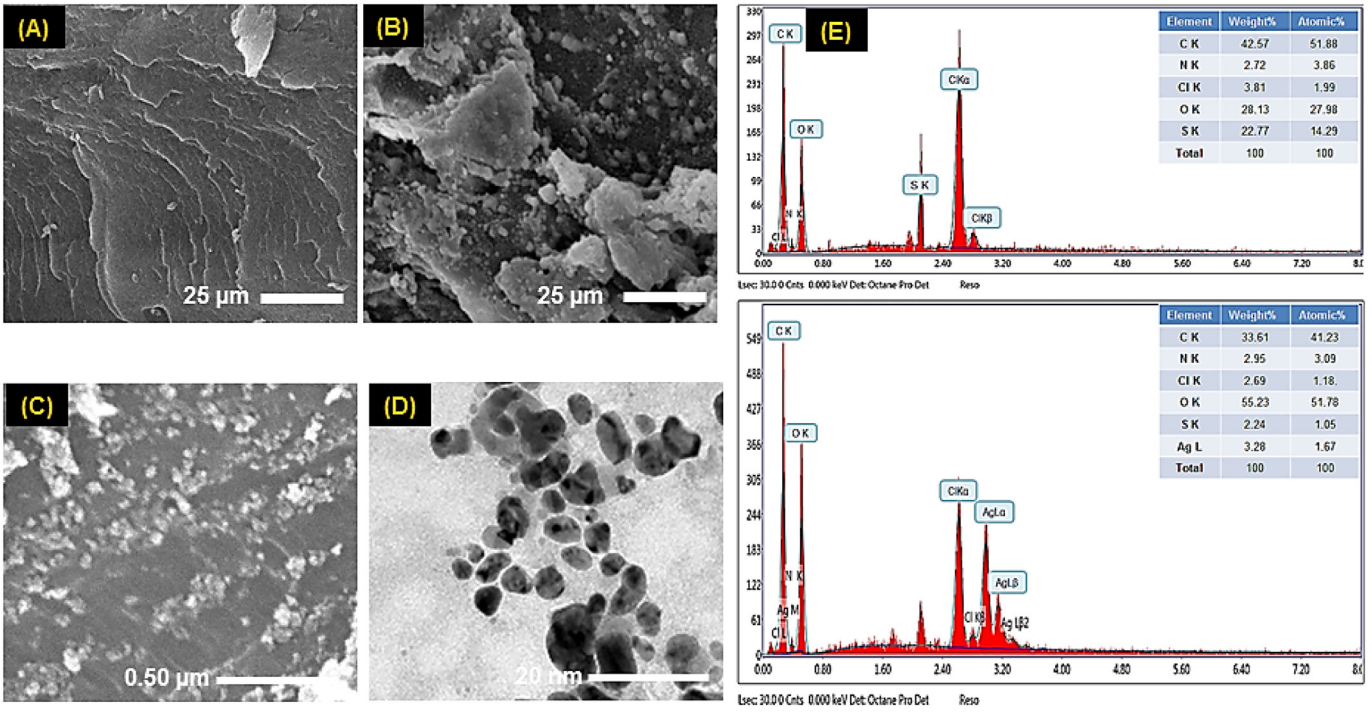

Fig. 4. (A,B,C) SEM micrographs of native MWSCT, Ag(I)MWSCT complex, and silver nano-composite (Ag(0)MWSCT), respectively. (D) TEM image of Ag(0)MWSCT. (E) EDX spectra of MWSCT (top) and Ag(0)MWSCT (bottom), respectively.

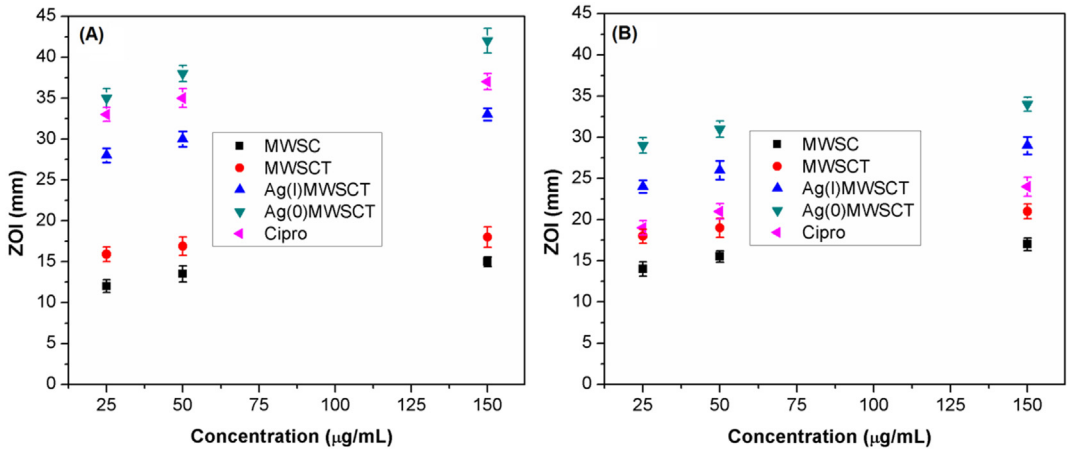

Fig. 5. Zone of inhibition (ZOI) values as markers of antibacterial activity of various synthesized materials in mm against (**A**) *E. coli* and (**B**) *S. aureus*.

materials have remarkable higher antibacterial efficacies, with a better effect against *E. coli*. Noteworthy, the nanosilver-MWSCT composite (Ag(0)MWSCT) ($ZOI_{E.\ coli} = 42–35$ mm; $ZOI_{S.\ aureus} = 34–29$ mm) has greater antibacterial effects complex than the silver(I)-MWSCT complex (Ag(I)MWSCT) ($ZOI_{E.\ coli} = 33–28$ mm; $ZOI_{S.\ aureus} = 29–24$ mm. The increased activity of silver-based MWSCT as compared to native MWSCT is due to the higher infiltration of the silver component and its capacity to induce multiple bactericidal effects into the bacterial cell including: (i) Disrupting the bacterial cell membrane via interaction with the bacterial envelope components; (ii) Malfunctioning in the bacterial cell through binding to biomolecules (functional proteins, nucleic acids, and enzymes) inside the cell; (iii) Catalyzing the production of reactive oxygen species (ROS) [55]. Meanwhile, the promoted activity of the silver nanocomposite in comparison to the silver complex can be attributed to the smaller size of the nanosilver particles allowing them to strongly interact and bind with the bacterial surface causing biological malfunctions within the bacterial cell [56]. The inhibition of signal transduction and consequently bacterial growth through signal transduction as a result of phosphorylation of tyrosine residues on the peptide substrates could offer a plausible explanation for the higher anti-*E. coli* activity as compared to anti-staphylococcal efficacy [55]. Moreover, the structural difference of bacterial wall in Gram-negative and Gram-positive bacteria may offer another reason for this preferable activity against *E. coli*. Additionally, the capping of nanosilver with chitosan thiomer enhances the bioadhesive feature of the colloidal system allowing facile diffusion of nanoparticles through the mucus-layer of bacterial species.

The AWD assay revealed that MWSCT-based silver architectures exhibit better antibacterial efficiencies compared to the native MWSCT and MWSC. Hence, further antibacterial studies were performed for these silver architectures only against the targeted bacterial strains. These studies were carried out based on the CFU method in which the CFU/mL values were estimated for both untreated samples of *E. coli* and *S. aureus* (growth controls) and bacterial samples treated with silver architectures. As aforementioned in the experimental section, the CFU/mL was found to be 19.3×10^6 and 21.5×10^6 CFU/mL for the controls of *S. aureus* and *E. coli*, respectively. As shown in Fig. 6A, a marked reduction in the proliferation of bacterial cells was observed in the bacterial samples treated with silver architectures as revealed from the lowering of CFU/mL values in these samples. Where the counts of *E. coli* and *S. aureus* were diminished to 1.9×10^5 (99.2% bacterial reduction compared to growth control) and 3.4×10^5 CFU/mL (98.2% bacterial reduction compared to growth control), respectively, in Ag(0) MWSCT-treated samples. On the other hand, in Ag(I)MWSCT-treated samples the colonization of bacterial cells were reduced by 95.3% and 94.8% for *E. coli* and *S. aureus*, respectively. Thus, the obtained data reveal that the proliferation of bacterial cells has significantly reduced upon treatment with MWSCT-based silver architectures. These results are in good consistency with those obtained by AWD method.

The minimum inhibitory concentrations (MICs) of the newly synthesized MWSCT-based silver architectures against *E. coli* and *S. aureus* were estimated by the broth dilution (BD) method. BD assay was carried out in 96-well microtiter plate using samples with concentrations range between 0.05 and 32 μg/mL. The MICs values (Fig. 6B) revealed that the bactericidal efficacy of Ag(0)MWSCT against *E. coli* ($MIC_{E.\ coli} =$

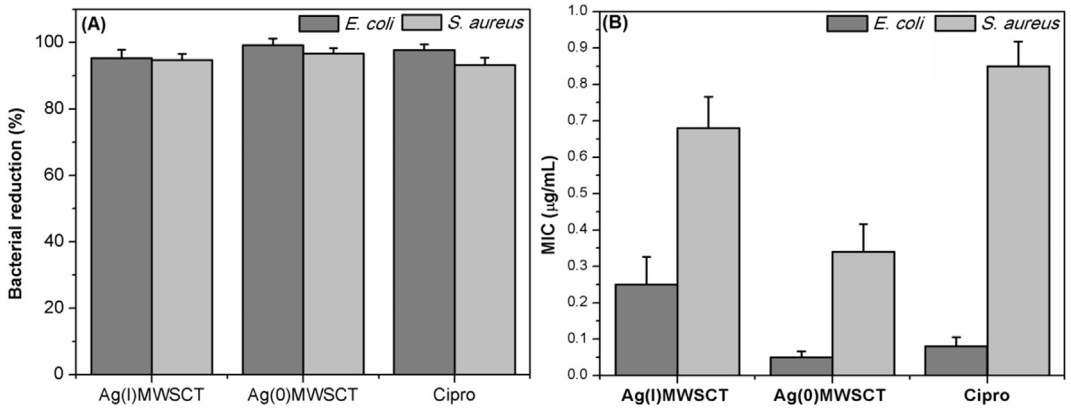

Fig. 6. (**A**) Effects of MWSCT-based silver architectures (Ag(I)MWSCT, Ag(0)MWSCT) on *E. coli* and *S. aureus* using CFU protocol; (**B**) The minimum inhibitory concentrations (MICs) values (μg/mL) of these silver derivatives against the targeted bacterial strains (*E. coli* and *S. aureus*) in comparison to ciprofloxacin HCl (Cipro) (positive control).

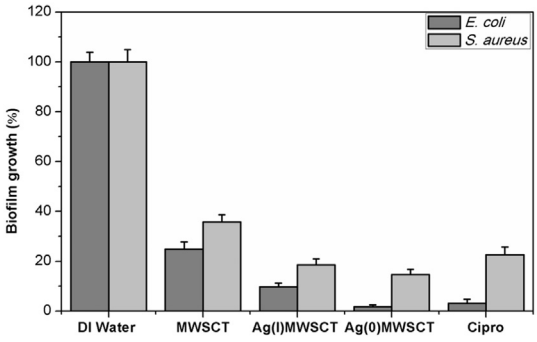

Fig. 7. Prevention of *E. coli* and *S. aureus* biofilms formation by MWSCT and its silver architectures (Ag(I)MWSCT, Ag(0)MWSCT) in comparison to Cipro as a positive control and DI water as a negative (untreated) control. Biofilm formation was quantified using crystal violet staining.

~0.05 μg/mL) was 5 and 1.6-times higher than that of Ag(I)MWSCT ($MIC_{E.\ coli}$ = 0.25 μg/mL) and Cipro ($MIC_{E.\ coli}$ = 0.08 μg/mL), respectively. Otherwise, the susceptibility of *S. aureus* toward silver architectures is lower than *E. coli*, where, the anti-staphylococcal activity of Ag(0)MWSCT ($MIC_{S.\ aureus}$ = 0.34 μg/mL) was 2 and 2.5-times higher than that of Ag(I)MWSCT ($MIC_{S.\ aureus}$ = 0.68 μg/mL) and Cipro ($MIC_{S.\ aureus}$ = 0.85 μg/mL), respectively. These results clarified that the Ag-MWSCT nano-composite manifested the lowest MICs values and thus the highest bactericidal efficiency against tested strains. This can be ascribed to the presence of thiol groups along with the smaller size of the nano-composite system leading to the higher monodispersibility and better bioavailability of silver in the nano-composite system.

3.5. Antibacterial biofilm assessment

The capacity of MWSCT and its silver architectures (Ag(I)MWSCT, Ag(0)MWSCT) to limit the formation of *E. coli* and *S. aureus* biofilms on polystyrene surfaces were in vitro assessed in comparison to the growth, negative (deionized water), and positive (Cipro) controls. As shown in Fig. 7, all the tested materials have the ability to strongly inhibit the bacterial biofilms formation, in a structure- and species-dependent manner, as compared to the controls. For instance, MWSCT can curb the staphylococcal biofilm formation more effectively than *E. coli* biofilm, while, the effect of silver architectures in the prevention of *E. coli* biofilm growth was greater than that against staphylococcal biofilm. It is clear that the biofilm production by a Gram-negative strain *E. coli* was significantly frustrated by MWSCT and its silver derivatives (Fig. 7). In particular, MWSCT-Ag nano-composite (Ag(0)MWSCT) showed the highest anti-*E. coli* biofilm effect (only 1.7% ± 0.75% biofilm growth) which was higher than that of positive control (Cipro) (3.1% ± 1.6% biofilm growth) (Fig. 7). Based on the aforementioned results, the higher activity of Ag(0)MWSCT to prevent *E. coli* biofilm formation could be attributed to inhibition of the adherence of *E. coli* cells onto the polystyrene surfaces coated with this nano-composite, coupled with its very potent antibacterial effect on the *E. coli* cells submerged in cultures or in biofilms.

Similarly, MWSCT and its silver architectures also showed inhibitory effects against staphylococcal biofilm formation, however, with lower efficacies in comparison to *E. coli*. In a similar trend, the order capacity in inhibiting the formation of staphylococcal biofilm is Ag(0)MWSCT (85.3% growth inhibition) > Ag(I)MWSCT (80.5% growth inhibition) > positive control (Cipro) (77.4% growth inhibition) > MWSCT (64.2% growth inhibition) (Fig. 7). Again, the antibiofilm performance is likely based on the banning of *S. aureus* cells to adhere to onto the polystyrene surfaces coated with the MWSCT or its silver derivatives, coupled with their higher bactericidal impacts of on the *S. aureus* cells submerged in cultures or in biofilms.

4. Conclusion

In this work, we have refined shrimp shell wastes to *N*-methylated water-soluble chitosan thiomer (MWSCT) which employed as a bioactive scaffold for ionic or elemental silver to fabricate MWSCT-based silver architectures (Ag(I)MWSCT, Ag(0)MWSCT). MWSCT was used as either a chelating agent for Ag(I) ions in order to form an Ag(I) MWSCT complex, or a bio-reductant and capping agent for Ag(I) ions in the preparation of a silver nano-composite Ag(0)MWSCT. The antibacterial and anti-biofilm performance of the new methylated chitosan thiomer (MWSCT) and its silver architectures (Ag(I)MWSCT, Ag(0) MWSCT) were in vitro assessed against *E. coli* and *S. aureus*. These new biopolymeric materials have significant ability to synergistically inhibit the proliferation of the targeted bacterial strain and prevent biofilm growth. Ag(0)MWSCT emerged as the most potent compound in inhibiting the growth of bacterial strains ($MIC_{E.\ coli}$/ $MIC_{S.\ aureus}$ = 0.05/0.34 μg/mL, 1.6−/ 2.5-times lower than that recorded for the clinical drug (ciprofloxacin, Cipro)). Also, this nano-composite showed the highest anti-biofilm effects (only 1.7% *E. coli* biofilm growth; 11.8% *staphylococcal* biofilm growth).

CRediT authorship contribution statement

Reda F.M. Elshaarawy: Conceptualization, Methodology, Data curation, Validation, Visualization, Writing - original draft, Writing - review & editing.**Lamia A. Ismail:**Conceptualization, Methodology, Writing - original draft.**Mohammad Y. Alfaifi:**Software, Data curation, Writing - original draft.**Moustafa A. Rizk:**Conceptualization, Methodology, Data curation, Writing - original draft.**Enas E. Eltamany:**Methodology, Data curation, Validation, Visualization, Writing - original draft. **Christoph Janiak:**Supervision, Writing - original draft, Writing - review & editing.

Appendix A. Supplementary data

Supporting information (experimental and spectral data) associated with this article is available with the article through the journal Web site, Supplementary data to this article can be found online at doi: https://doi.org/10.1016/j.ijbiomac.2020.02.284.

References

[1] G. Gebreyohannes, A. Nyerere, C. Bii, D.B. Sbhatu, Challenges of intervention, treatment, and antibiotic resistance of biofilm-forming microorganisms, Heliyon 5 (8) (2019), e02192. https://doi.org/10.1016/j.heliyon.2019.e02192.
[2] P. Lens, A.P. Moran, T. Mahony, P. Stoodley, V. O'Flaherty, Biofilms in Medicine, Industry and Environmental Biotechnology: Characteristics, Analysis and Control Published by IWA Publishing, Alliance House, London SW1H 0QS, UK, 2003.
[3] W. Yin, Y. Wang, L. Liu, J. He, Biofilms: the microbial "protective clothing" in extreme environments, Int. J. Mol. Sci. 20 (14) (2019) 3423, https://doi.org/10.3390/ijms20143423.
[4] N. Hoiby, T. Bjarnsholt, M. Givskov, S. Molin, O. Ciofu, Antibiotic resistance of bacterial biofilms, Int. J. Antimicrob. Agents 35 (2009) 322-332. DOI: https://doi.org/10.1016/j.ijantimicag.2009.12.011.
[5] I. Kolodkin-Gal, S.G. Cao, L. Chai, T. Böttcher, R. Kolter, J. Clardy, R. Losick, A self-produced trigger for biofilm disassembly that targets exopolysaccharide. Cell 149 (2012) 684-692. DOI: https://doi.org/10.1016/j.cell.2012.02.055.
[6] O.E. Petrova, K.E. Cherny, K. Sauer, The diguanylate cyclase GcbA facilitates *Pseudomonas aeruginosa* biofilm dispersion by activating BdlA, J. Bacteriol. 197 (2015) 174-187. DOI: https://doi.org/10.1128/JB.02244-14.
[7] S. Yu, T.T. Su, H.J. Wu, S.H. Liu, D. Wang, T.H. Zhao, Z.J. Jin, W.B. Du, M.J. Zhu, S.L. Chua, L. Yang, D.Y. Zhu, L.C. Gu, L Z. Ma, PslG, A self-produced glycosyl hydrolase, triggers biofilm disassembly by disrupting exopolysaccharide matrix. Cell Res. 25 (2015) 1352-1367. DOI: https://doi.org/10.1038/cr.2015.129.
[8] R. Canaparo, F. Foglietta, F. Giuntini, C.D. Pepa, F. Dosio, L. Serpe, Recent developments in antibacterial therapy: focus on stimuli-responsive drug-delivery systems and therapeutic nanoparticles, Molecules 24 (2019) (1991) https://doi.org/10.3390/molecules24101991.
[9] K.R. Sims, Y. Liu, G. Hwang, H.I. Jung, H. Koo, D.S.W. Benoit, Enhanced design and formulation of nanoparticles for anti-biofilm drug delivery, Nanoscale 11 (1) (2018) 219–236, https://doi.org/10.1039/c8nr05784b.

[10] A.L.Z. Lee, V.W.L. Ng, W.X. Wang, J.L. Hedrick, Y.Y. Yang, Block copolymer mixtures as antimicrobial hydrogels for biofilm eradication, Biomaterials 34 (2013) 10278-10286. DOI: https://doi.org/10.1016/j.biomaterials.2013.09.029.

[11] Y. Jiao, F.R. Tay, L. Niu, J. Chen, Advancing antimicrobial strategies for managing oral biofilm infections, Int. J. Oral Sci. 11 (2019) 28, https://doi.org/10.1038/s41368-019-0062-1.

[12] Y.D. Boakye, N. Osafo, C.A. Danquah, F. Adu, C. Agyare, Antimicrobial Agents: Antibacterial Agents, Anti-Biofilm Agents, Antibacterial Natural Compounds, and Antibacterial Chemicals, IntechOpen, 2019https://doi.org/10.5772/intechopen.82560.

[13] E. Galdiero, L. Lombardi, A. Falanga, G. Libralato, M. Guida, R. Carotenuto, Biofilms: novel strategies based on antimicrobial peptides, Pharmaceutics 11 (2019) 322, https://doi.org/10.3390/pharmaceutics11070322.

[14] M. K. Rai, S.D. Deshmukh, A.P. Ingle, A.K. Gade, Silver nanoparticles: the powerful nanoweapon against multidrug-resistant bacteria, J. Appl. Microbiol. 112 (2012) 841-852. DOI: https://doi.org/10.1111/j.1365-2672.2012.05253.x.

[15] G. Franci, A. Falanga, S. Galdiero, L. Palomba, M. Rai, G. Morelli, M. Galdiero, Silver nanoparticles as potential antibacterial agents, Molecules 20 (5) (2015) 8856–8874, https://doi.org/10.3390/molecules20058856.

[16] S. Nakamura, M. Sato, Y. Sato, N. Ando, T. Takayama, M. Fujita, M. Ishihara, Synthesis and application of silver nanoparticles (AgNPs) for the prevention of infection in healthcare workers, Int. J. Mol. Sci. 20 (2019) 3620, https://doi.org/10.3390/ijms20153620.

[17] M. Catauro, M.G. Raucci, F.D. de Gaetano, A. Marotta, Antibacterial and bioactive silver-containing Na2Ox·CaOx·2SiO2 glass prepared by sol-gel method, J. Mater. Sci.: Mater. Med. 15 (2004) 831-837. DOI: https://doi.org/10.1023/b:jmsm.0000032825.51052.00.

[18] J.H. Crabtree, R.J. Burchette, R.A. Siddiqi, I.T. Huen, L.L. Handott, A. Fishman, The efficacy of silver-ion implanted catheters in reducing peritoneal dialysis-related infections, Peritoneal Dial. Int. 23 (2003) 368–374.

[19] S.H. Mohammed, M.S. Mahdi, A.M. Bashi, M.M. Ahmed, Simultaneous antibacterial and antibiofilm activities of three types of silver nanoparticles against human bacterial pathogens, Int. J. Pharmaceut. Qual. Assur. 10 (1) (2019) 119–127, https://doi.org/10.25258/ijpqa.10.1.19.

[20] H.-J. Park, S. Park, J. Roh, S. Kim, K. Choi, J. Yi, Y. Kim, J. Yoon, Biofilm-inactivating activity of silver nanoparticles: A comparison with silver ions, J. Ind. Eng. Chem. 19 (2013) 614-619. DOI: https://doi.org/10.1016/j.jiec.2012.09.013.

[21] C.-Y. Loo, P.M. Young, R. Cavaliere, C.B. Whitchurch, W.-H. Lee, R. Rohanizadeh, Silver nanoparticles enhance *Pseudomonas aeruginosa* PAO1 biofilm detachment, Drug Dev. Ind. Pharm., 40 (2014) 719-729. DOI: https://doi.org/10.3109/03639045.2013.780182.

[22] G.A. Martinez-Castanon, N. Nino-Martinez, F. Martinez-Gutierrez, J.R. Martinez-Mendoza, F. Ruiz, Synthesis and antibacterial activity of silver nanoparticles with different sizes, J. Nanopart. Res. 10 (2008) 1343-1348. DOI: https://doi.org/10.1007/s11051-008-9428-6.

[23] M.J. Ruben, E.J. Luis, C. Alejandra, H. Katherine, B.K. Juan, R.J. Tapia, Y.M. Jose, The bactericidal effect of silver nanoparticles, Nanotechnol. 16 (2005) 2346, https://doi.org/10.1088/0957-4484/16/10/059/meta.

[24] S. Chernousova, M. Epple, Silver as antibacterial agent: Ion, Nanoparticle, and Metal. Angew. Chem., Int. Ed. 2013, 52, 1636-1653. DOI: https://doi.org/10.1002/anie.201205923.

[25] S. Leon-Silva, F. Fernandez-Luqueno, F. Lopez-Valdez, Silver nanoparticles (AgNPs) in the environment: A review of potential risks on human and environmental health. Water Air Soil Pollut. 227 (2016) 306-225. DOI: https://doi.org/10.1007/s11270-016-3022-9.

[26] H.M. Fahmy, A.M. Mosleh, A. Abd Elghany, E. Shams-Eldin, E.S. Abu Serea, S.A. Alia, A.E. Shalan, Coated silver nanoparticles: synthesis, cytotoxicity, and optical properties, RSC Adv. 9 (2019) 20118-20136. DOI: https://doi.org/10.1039/C9RA02907A.

[27] V.K.H. Bui, D. Park, Y.-C. Lee, Chitosan combined with ZnO, TiO2 and Ag nanoparticles for antimicrobial wound healing applications: a mini review of the research trends, Polymers 9 (2017) 1–24, https://doi.org/10.3390/polym9010021.

[28] N. Kahya, Water-soluble chitosan derivatives and their biological activities: a review, Polym. Sci. 5 (1) (2019) 3.

[29] Y.-J. Jeon, P.-J. Park, S.-K. Kim, Antimicrobial effect of chitooligosaccharides produced by bioreactor, Carbohydr. Polym. 44 (2001) 71–76, https://doi.org/10.1016/S0144-8617(00)00200-9.

[30] N. Rakkhumkaew, C. Pengsuk, Chitosan and chitooligosaccharides from shrimp shell waste: characterization, antimicrobial and shelf life extension in bread, Food Sci. Biotechnol. 27 (4) (2018) 1201–1208, https://doi.org/10.1007/s10068-018-0332-2.

[31] M. Zhao, L. Gu, Y. Li, S. Chen, J. You, L. Fan, Y. Wang, L. Zhao, Chitooligosaccharides display anti-tumor effects against human cervical cancer cells via the apoptotic and autophagic pathways, Carbohydr. Polym. 224 (2019) 115171. DOI: https://doi.org/10.1016/j.carbpol.2019.115171.

[32] R.L. Xing, S. Liu, Z.Y. Guo, H. Yu, P. Wang, C. Li, Z. Li, P. Li, Relevance of molecular weight of chitosan and its derivatives and their antioxidant activities in vitro, Bioorg. Med. Chem. 13 (2005) 1573-1577. DOI: https://doi.org/10.1016/j.bmc.2004.12.022.

[33] T. Sun, D.X. Zhou, J.L. Xie, F. Mao, Preparation of chitosan oligomers and their antioxidant activity, Eur. Food Res. Technol. 225 (2007) 451-456. DOI: https://doi.org/10.1007/s00217-006-0439-1.

[34] R. Kalaivani, M. Maruthupandy, T. Muneeswaran, A.H. Beevi, M. Anand, C.M. Ramakritinan, A.K. Kumaraguru, Synthesis of chitosan mediated silver nanoparticles (Ag NPs) for potential antimicrobial applications, Frontiers in Laboratory Medicine 2 (2018) 30–35, https://doi.org/10.1016/j.flm.2018.04.002.

[35] U. Latif, K. Al-Rubeaan, A.T.M. Saeb, A review on Antimicrobial Chitosan-Silver Nanocomposites: A Roadmap Toward Pathogen Targeted Synthesis International Journal of Polymeric Materials and Polymeric Biomaterials, 64: 2014 448–458. DOI: https://doi.org/10.1080/00914037.2014.958834.

[36] R.F.M. Elshaarawy, A.A. Refaee, E.A. El-Sawi, Pharmacological performance of novel poly-(ionic liquid)-grafted chitosan-N-salicylidene Schiff bases and their complexes, Carbohydr. Polym. 146 (2016) 376-387. DOI: https://doi.org/10.1016/j.carbpol.2016.03.017.

[37] R.F.M. Elshaarawy, F.H.A. Mustafa, A. Herbst, A.E.M. Farag, C. Janiak, Surface functionalization of chitosan isolated from shrimp shells, using salicylaldehyde ionic liquids in exploration for novel economic and ecofriendly antibiofoulants, RSC Adv. 6 (2016) 20901-20915. DOI: https://doi.org/10.1039/C5RA27489C.

[38] A.R. Sofy, A.A. Hmed, N.F. Abd El Haliem, M.A.-E. Zein, R.F.M. Elshaarawy, Polyphosphonium-oligochitosans decorated with nanosilver as new prospective inhibitors for common human enteric viruses. Carbohydr. Polym. 226 (2019) 115261. DOI: https://doi.org/10.1016/j.carbpol.2019.115261.

[39] K. Chauhan, R. Sharma, R. Dharela, G.S. Chauhan, R.K. Singhal, Chitosan-thiomer stabilized silver nanocomposites for antimicrobial and antioxidant applications, RSC Adv. 6 (2016) 75453–75464. DOI: https://doi.org/10.1039/c6ra13466a.

[40] C. Perez, P.M. Bazerque, An antibiotic assay by agar well diffusion method, Acta Biol. Med. Exp. 15 (1990) 113–115.

[41] R.F.M. Elshaarawy, F.H.A. Mustafa, L. van Geelen, A.E.A. Abou-Talebe, H.R.Z. Tadrose, R. Kalscheuerd, C. Janiak, Mining marine shell wastes for polyelectrolyte chitosananti-biofoulants: Fabrication of high-performance economic and ecofriendly anti-biofouling coatings, Carbohydr. Polym. 172 (2017) 352–364. DOI: https://doi.org/10.1016/j.carbpol.2017.05.059.

[42] G.D. Christensen, W.A. Simpson, J.J. Younger, L.M. Baddour, F.F. Barrett, D.M. Melton, E.H. Beachey, Adherence of coagulase-negative staphylococci to plastic tissue culture plates: a quantitative model for the adherence of staphylococci to medical devices, J. Clin. Microbiol. 22 (6) (1985) 996–1006.

[43] M. Wu, Z. Long, H. Xiao, C. Dong, Preparation of N, N, N-trimethyl chitosan via a novel approach using dimethyl carbonate, Carbohydr. Polym. 169 (2017) 83–91, https://doi.org/10.1016/j.carbpol.2017.03.043.

[44] K. Chauhan, P. Singh, R.K. Singhal, New chitosan−thiomer: an efficient colorimetric sensor and effective sorbent for mercury at ultralow concentration, ACS Appl. Mater. Interfaces 7 (47) (2015) 26069–26078, https://doi.org/10.1021/acsami.5b06078.

[45] M.R. Kasaai, J. Arul, G. Charlet, Intrinsic viscosity–molecular weight relationship for chitosan, J. Polym. Sci. 38 (19) (2000) 2591–2598, https://doi.org/10.1002/1099-0488(20001001)38:19<2591:AID-POLB110>3.0.CO;2-6.

[46] J.-W. Nah, M.-K. Jang, Spectroscopic characterization and preparation of low molecular, water-soluble chitosan with free-amine group by novel method, J. Polymer Sci. A 40 (21) (2002) 3796–3803, https://doi.org/10.1002/pola.10463.

[47] D. de Britto, O.B.G. Assis, A novel method for obtaining a quaternary salt of chitosan, Carbohydr. Polym. 69 (2) (2007) 305–310, https://doi.org/10.1016/j.carbpol.2006.10.007.

[48] B. Narayana, M.R. Gajendragad, Complexes of Zn(II), Pd(II), Hg(II), Pb(II), Cu(I), Ag (I) and Tl(I) with 4-amino-5-mercapto-3-(0-tolyloxymethyl)-1,2,4-triazole, Tr. J. Chem. 21 (1997) 71–76.

[49] R.F.M. Elshaarawy, G.A. Seif, M.E. El-Naggar, T.B. Mostafa, E.A. El-Sawi, In-situ and ex-situ production of poly-(imidazolium vanillyl)-grafted chitosan/silver nanobiocomposites for eco-friendly antibacterial finishing of cotton fabrics, Eur. Polymer J. 116 (2019) 210-221. DOI: https://doi.org/10.1016/j.eurpolymj.2019.04.013.

[50] E. Curti, D. de Britto, S.P. Campana-Filho, Methylation of chitosan with iodomethane: effect of reaction conditions on chemoselectivity and degree of substitution, Macromol. Biosci. 3 (10) (2003) 571–576, https://doi.org/10.1002/mabi.200300030.

[51] C.Y. Won, C.C. Chu, T.J. Yu, Synthesis of starch-based drug carrier for the control/ release of Estrone hormone, Carbohydr. Polym. 32 (1997) 239−244. DOI: https://doi.org/10.1016/S0144-8617(96)00169-5.

[52] M. Farrag, M. Thamer, M. Tschurl, T. Bürgi, U. Heiz, Preparation and spectroscopic properties of monolayer-protected silver nanoclusters, J. Phys. Chem. C 116 (2012) 8034-8043. DOI: https://doi.org/10.1021/jp210453v.

[53] D. K. Boz˘anic, L.V. Trandafilovic, A.S. Luyt, V. Djokovic, Green synthesis and optical properties of silver–chitosan complexes and nanocomposites, React. Funct. Polym. 70 (2010) 869–873. DOI: https://doi.org/10.1016/j.reactfunctpolym.2010.08.001.

[54] P. Mulvaney, Surface Plasmon Spectroscopy of nanosized metal particles. Langmuir, 12 (1996) 788-800. DOI: https://doi.org/10.1021/la9502711.

[55] A. Kędziora, M. Speruda, E. Krzyżewska, J. Rybka, A. Łukowiak, G. Bugla-Płoskońska, Similarities and differences between silver ions and silver in nanoforms as antibacterial agents, Int. J. Mol. Sci. 19 (2) (2018) 444, https://doi.org/10.3390/ijms19020444.

[56] K. Zawadzka, K. Kadzioła, A. Felczak, N. Wronska, I. Piwonski, A. Kisielewska, K. Lisowska, Surface area or diameter – which factor really determines the antibacterial activity of silver nanoparticles grown on TiO2 coatings?, New J. Chem. 38 (2014) 3275-3281. DOI: https://doi.org/10.1039/C4NJ00301B.